Research Article Vol. 33, No. 8 / 21 Apr 2025 / Optics Express 17233
Optics EXPRESS

SMNS structure based fiber optic interferometer for cadmium detection

XUJIE WANG,[1] ABDULLAH AL NOMAN,[2,3] YIFAN LIU,[1] AND CHANGYUAN YU[1,*]

[1]*Photonics Research Center, Department of Electronic and Electrical Engineering, The Hong Kong Polytechnic University, 11 Yuk Choi Rd., Hung Hom 999077, Hong Kong SAR, China*
[2]*Department of Electronic and Computer Engineering, University of Limerick, Castletroy, Co. Limerick V94 EY04, Ireland*
[3]*abdullah.noman@ul.ie*
[*]*changyuan.yu@polyu.edu.hk*

Abstract: A cost-effective, easy-to-manufacture, compact, and reliable single-mode fiber/ multimode fiber/ no-core fiber/ single-mode fiber (SMNS) structure based interferometer is proposed for the detection of cadmium ions (Cd^{2+}). This setup involves splicing a segment of multimode fiber (MMF) and no-core fiber (NCF) between a single-mode fiber (SMF), followed by a functionalization procedure with a composite of graphene oxide (GO)-cysteamine (MEA) and chitosan (CS)-Cd^{2+} imprinted polymer (Cd^{2+}IP). The sensitivity of the sensors has been calculated by monitoring the interference minima. Three identical probes have been fabricated to ensure the duplicability and the highest sensing sensitivity is measured at -0.1211 nm/ parts per billion (ppb) in the cadmium detection range of 0 ppb to 10 ppb with a response time of 90 s. The probe demonstrates a high selectivity for Cd^{2+} compared to other heavy metal ions. The response of the probe in various pH solutions has been investigated to minimize the sensing error. Further, the temperature crosstalk is eliminated by assessing the response of a fiber Bragg grating (FBG).

1. Introduction

Heavy metal elements (such as lead, arsenic, cadmium, mercury, etc.) pose significant risks to both human health and the environment with extensive toxicity and bioaccumulation potential over the year [1]. Cadmium (Cd) is considered one of the most toxic metal ions due to its numerous harmful effects on human health (e.g., hypertension, cardiovascular and cerebrovascular disorders, etc.) [2]. Therefore, the World Health Organization (WHO) has stringent limits for Cadmium concentration in drinking water and in-situ water up to 3 parts per billion (ppb) [3]. Various conventional approaches have been followed to detect cadmium in water, such as atomic absorption spectrometry (AAS), inductively coupled plasma mass spectrometry (ICP-dS), X-ray fluorescence spectroscopy (XRF), electrochemical, chemiluminescence, and spectrophotometry [4–8]. However, these techniques either require expensive equipment (AAS, ICP-MS, XRF), experience low accuracy due to sample pre-treatment (electrochemical method), or suffer from poor selectivity (chemiluminescence, spectrophotometry) [1,9,10]. Meanwhile, optical fiber based heavy metal ions (HMIs) sensing has gained attention due to their affordability, ease of use, selectivity, high sensitivity, antimagnetic resistance and integration capabilities [11–13].

Fiber optic sensors are primarily categorized into surface plasmon resonance (SPR), fluorescence, Raman and interferometric sensors depending on their sensing principle [14–18]. Whereas, interferometric method based fiber optic sensors have received substantial interest due to their adjustable observation wavelength, strong signals, and minimal susceptibility to interference [19]. Various techniques have been employed for Cd^{2+} detection using fiber optic interferometric sensors. For instance, Pan *et al.* demonstrated a 1-allyl-2 thiourea (ATU) and N,N'-Methylenebisacrylamide (BIS) modified fused-cone single-mode fiber (SMF) for cadmium

#547717 https://doi.org/10.1364/OE.547717
Journal © 2025 Received 21 Nov 2024; revised 27 Jan 2025; accepted 11 Feb 2025; published 10 Apr 2025

Optics EXPRESS

detection in 2019 [20]. The sensor achieved a detection limit of 4×10^{-7} mol/L, a sensitivity of 5.126×10^4 nm/(mol/L) with a measurement range of 0 mol/L to 1.2×10^{-5} mol/L. However, the sensor has low sensitivity and no selectivity. Xie *et al.* recently reported cadmium sensing based on a polyvinyl alcohol (PVA)/tetraethyl orthosilicate (TEOS)/3-aminopropyl triethoxysilane (APTES) film coated three-core optical fiber [21]. The sensor exhibited a linear sensitivity and detection limit of 7 nm/μM and 0.0143 μM, respectively. The sensitivity was demonstrated in the cadmium concentration range of 0 μM to 0.4 μM. Additionally, in 2024, Li *et al*. displayed an etched thin core fiber (TCF) section coated with ATU to detect a similar analyte and the sensor detection limit was recorded as 2.37×10^{-11} over a range of 0 mol/L to 1.2×10^{-9} mol/L [22]. All these abovementioned sensor constraints can be addressed by introducing the molecular imprinting technique (MIT). This technique creates receptors with highly specific binding sites that match the shape of the target molecule, ensuring accurate detection. By replacing the template molecule with ions like Cd^{2+}, the Cd^{2+}-imprinted polymer (Cd^{2+}IP) can be effectively used to detect cadmium in water-based media [23]. In addition to its high selectivity, this method provides benefits such as excellent stability, cost-effectiveness, fast response and robustness in challenging environments which makes it ideal for various sensing applications [24,25].

The aim of this study is to develop a compact and highly selective single-mode fiber/ multimode fiber/ no-core fiber/ single-mode fiber (SMNS) structure based fiber optic interferometer for cadmium ions sensing. The sensor fabrication process involves the fusion of multimode fiber (MMF) and No-core fiber (NCF) in between single-mode fiber (SMF). The section of NCF is coated with cysteamine-modified graphene oxide (GO-MEA) and chitosan (CS)-Cd^{2+}IP membranes to detect cadmium ions and ensure high selectivity. The GO-MEA captures trace Cd^{2+} through cation exchange and electrostatic attraction [26]. The coated layer also binds with MEA's thiol (-SH) and amino (-NH_2) groups [27]. The repeatability, response in different pH levels and detection time of the sensor are recorded to enhance the sensor accuracy. Furthermore, a small segment of fiber Bragg grating (FBG) has been added to the SMNS structure to minimize the measurement error due to cross temperature sensitivity.

2. Sensing principle, fabrication and performance of SMNS structure

2.1. Sensing principle

Figure 1 shows the schematic of the proposed sensor along with light distribution. The fundamental mode of the SMF undergoes diffraction at the SMF-MMF fused region when the light is transmitted into the SMF, leading to the simultaneous excitation of both the core and cladding modes in the MMF. The light further travels through the MMF and excites higher-order modes in the cladding region of NCF upon reaching at the MMF-NCF area. Where any changes in the outer environment can easily be detected due to the sensitive evanescent wave of the NCF cladding region [28,29]. Finally, the optical signal is coupled to the lead-out SMF and the interference spectrum is formed by accumulating phase alteration [30]. It can be noticed that the output light intensity increases with the excitation of the NCF cladding modes at the MMF-NCF junction. Thus, assuming the optical field of mth-order mode denotes by $\emptyset_m(r)$, r is the light path, the excitation coefficient of $\emptyset_m(r)$ denotes by b_m, and the propagation constant is β_m, during the light coupling into MMF with a distance of L, the filed distribution $E(r, L)$ can be expressed as [31]:

$$E(r, L) = \Sigma_{m=1}^{M} b_m \emptyset_m(r) \exp(j\beta_m L) \tag{1}$$

The amplitude $E_m(r)$ and light intensity I_m of the mth cladding mode at the NCF end can be defined as:

$$E_m(r) = b_m \emptyset_m \exp(j\beta_m L) \tag{2}$$

$$I_m = |E_m^*(r) E_m(r)| \tag{3}$$

Optics EXPRESS

The interference intensity between the core mode and the cladding modes can be described by Eq. (4), where I_{CO} and I_{Cl} are the intensities of the core and cladding modes, respectively. Also, the phase difference between the two modes ($\Delta\varphi$) depends on the effective refractive index difference between the core and cladding modes (Δn_{eff}), and the wavelength of the incident light λ.

$$I = I_{co} + I_{cl} + 2\sqrt{I_{co}I_{cl}}\cos(\Delta\varphi) \tag{4}$$

$$\Delta\varphi = \frac{2\pi L\Delta n_{eff}}{\lambda} \tag{5}$$

Therefore, mth-order interference minima λ_{md} along with the wavelength shift caused by cladding effective refractive index change Δn is expressed as:

$$\lambda_{md} = \frac{2\Delta n_{eff}L}{2N+1}, N = 0, 1, 2\ldots \tag{6}$$

$$\Delta\lambda_{md} = \frac{2\Delta nL}{2N+1}, N = 0, 1, 2\ldots \tag{7}$$

Thus, the interference fringes of the SMNS interferometer vary with ambient refractive index, enabling the detection of refractive index changes external to the NCF.

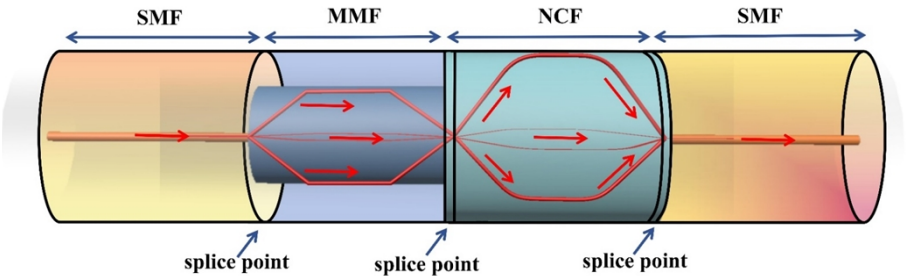

Fig. 1. Schematic diagram of SMNS structure based fiber optic cadmium sensor.

2.2. *Interferometer fabrication and refractive index sensitivity measurement*

The length of the MMF and NCF were optimized to enhance the SMNS structure sensitivity. In this way, firstly, the interference spectra were observed by following the experimental setup corresponding to different lengths of NCF in the single-mode fiber/ no-core fiber/ single-mode fiber (SNS) structure (see Fig. 2(a)). The length was initiated from 10 mm to 35 mm with a step of 5 mm. The optimal interference pattern can be observed with the 25 mm of NCF length due to the accumulated phase differences from numerous cladding modes. Subsequently, the length of MMF was adjusted in line with NCF to examine the transmitted spectra of the SMNS structure, as illustrated in Fig. 2(b). It can be seen that the MMF lengths shorter than 25 mm produced multiple wavelets in the interference spectra indicating the excitation of higher-order modes without significant phase differences. Besides, excessive loss and distorted waveforms were detected with MMF lengths beyond 25 mm. The frequency domain analysis in Fig. 2(c) showed that SMNS structures excited stronger main cladding modes compared to SNS, where the 25 mm-25 mm MMF-NCF splicing length resulted in the most optimal interference and mode intensity. The optical energy distribution is investigated by the beam propagation technique of RSOFT for SMNS arrangements. The simulated result was displayed in Fig. 2(d), where a length of 0.5 mm SMF (8.2 μm/125 μm), 25 mm MMF (60 μm/125 μm) and 25 mm NCF (125 μm) in line with the experimental optimization parameters were considered.

Optics EXPRESS

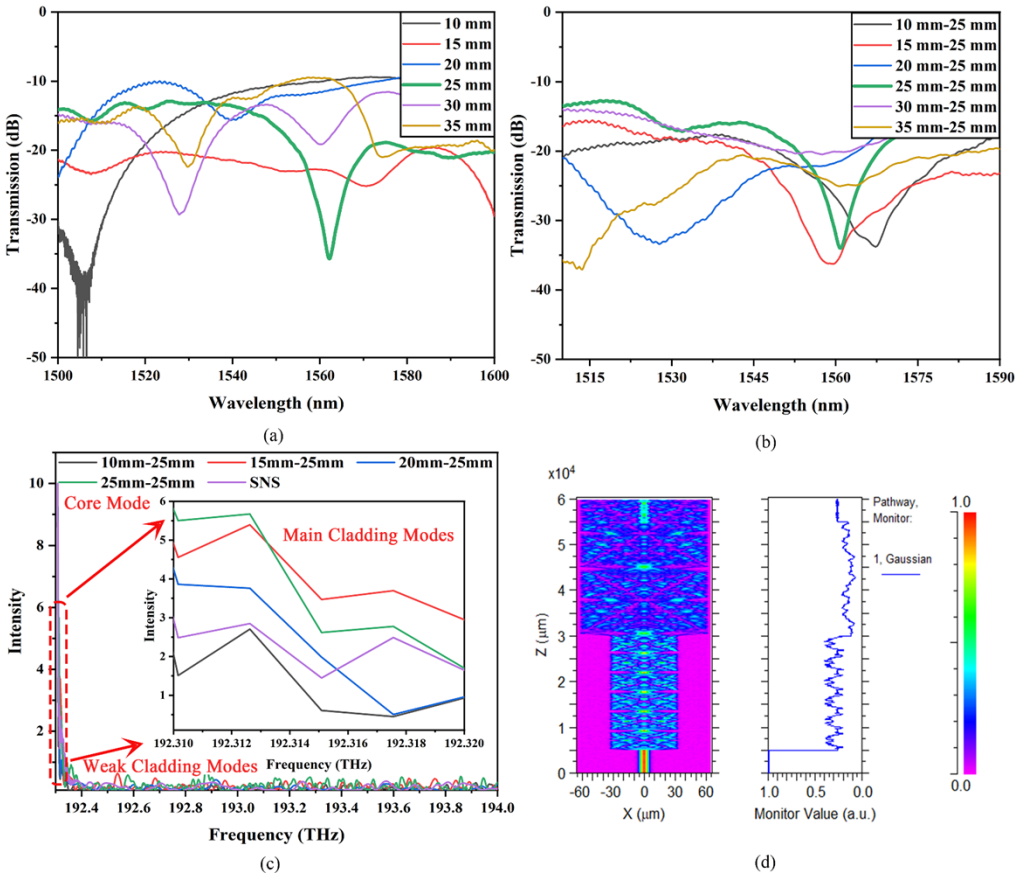

Fig. 2. Length optimization of NCF (a) and MMF-NCF (b) for the SMNS structure, (c) frequency analysis of different length based SMNS sensors, (d) optical field distribution of optimized SMNS length.

The graphical representation of the experimental arrangement is shown in Fig. 3. Wherein, one side of the SMNS interferometer was connected to a broadband source (BBS) with a power of 7.8 mW and an optical spectra analyzer (OSA, AQ6370D, YOKOGAWA, Tokyo, Japan) with a static spectral resolution of 0.02 nm on the other end. The BBS launched the incident light beam into the SMF to excite the cladding modes in the NCF. The OSA observed the transmitted SMNS spectrum was generated due to the interaction between the cladding modes and the surrounding atmosphere, leading to a wavelength shift. Besides, a section of FBG was inserted to monitor ambient temperature in follow-up work.

In addition, the effectiveness of the bare SMNS structure in response to the ambient environment was evaluated by immersing it in glycerol solutions with refractive indices (RIs) ranging from 1.3320 to 1.4235. The refractive indices of these solutions were measured using a digital refractometer (AIPLI, Shenzhen, China) after being prepared by mixing different concentrations of glycerol with deionized (DI) water. The minima of the bare SMNS sensor displayed a red shift in Fig. 4 with the increase in the refractive index (RI) of glycerol solutions. This shift happened due to the interaction between the cladding modes and the specific refractive index solution, resulting in a change in the effective index of the cladding modes. The response towards the several glycerol mixed RI solutions was recorded based on the previously described experimental setup. Additionally, two bare SMNS structure sensors were fabricated using similar physical

Optics EXPRESS

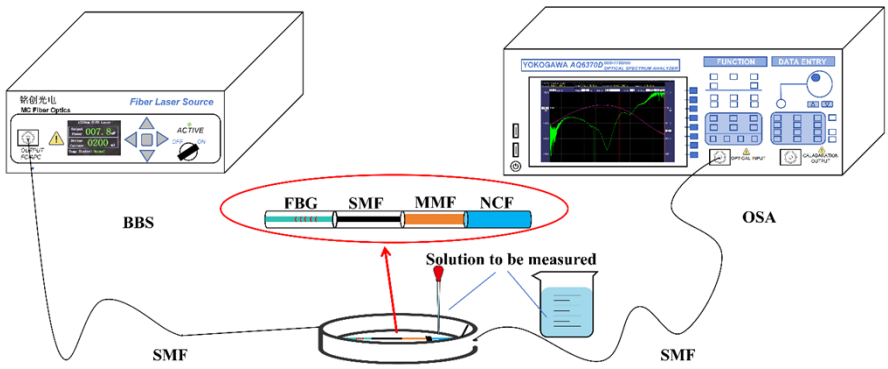

Fig. 3. Experimental setup for cadmium sensing.

criteria. All probes demonstrated a linear response and a comparable sensitivity of over 190 nm/refractive index unit (RIU) across various glycerol RI concentrations and the sensitivity to Cd^{2+} was further explored by functionalizing these probes in subsequent experiments.

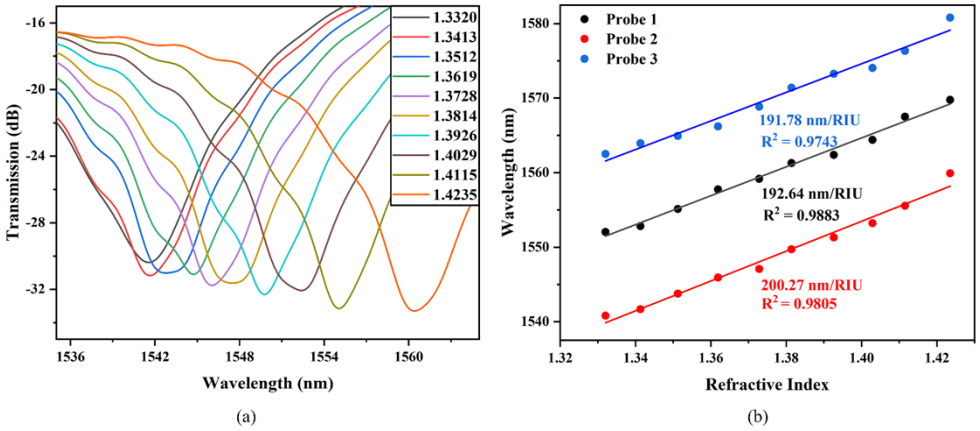

Fig. 4. (a) Interference minima movement (Probe 2) observed by immersing the bare SMNS structure in glycerol solutions with refractive indices ranging from 1.3320 to 1.4235. (b) The average sensitivity of the three fabricated probes towards the same the same range of glycerol concentrations.

3. Sensor functionalization

3.1. Reagents

The chemical materials utilized for the proposed interferometer functionalization include GO, MEA, N-(3-Dimethylaminopropyl)-N-ethylcarbodiimide (EDC), N-hydroxybutanediimide (NHS), Phosphate-Buffered Saline (PBS), CS, acetic acid, epichlorohydrin (ECH), ethylene diamine tetraacetic acid (EDTA), Cadmium chloride, Zinc chloride, Copper nitrate trihydrate, Mercury nitrate monohydrate, Chromium nitrate nonahydrate, Sodium hydroxide. All these materials were used for the fabrication process without any extra modification and purchased directly from Sigma Aldrich. In addition, the solvent for all the HMIs was prepared by using DI water.

Optics EXPRESS

3.2. Sensor functionalization

The coating procedure was separated into two stages to make the sensors sensitive to the Cd^{2+}, as depicted in Fig. 5(a). In the first stage, the fabricated probe was coated with the GO-MEA membrane layer (see Fig. 5(b)). In this process, the fiber was thoroughly cleaned with ethanol to remove the dust from the fiber surface. The fiber was then immersed in 1 mg/L GO dispersion for 30 mins, followed by baking at 55 °C for two hours to achieve a uniform coating on the NCF surface. This coating process was repeated three times to grow the negatively charged oxygen containing groups (OCGs), facilitating the electrostatic adsorption of Cd^{2+}. Consequently, the GO modified probe was treated within a mixed solution of EDC and NHS for 20 mins. The solution was prepared by adding 0.1 mol/L NHS into 0.4 mol/L EDC. The probe was further drenched in PBS solutions for 30 mins to activate the carboxyl group (-COOH) in OCGs. In order to complete the GO-MEA coating layer, the probe was submerged in a 10 mM MEA solution for self-assembly of MEA via amide bonds (-CO-NH-) [32]. The probe was again dried at 55 °C in a temperature chamber, creating amide and thiol groups on the fiber surface to enhance sensitivity to cadmium ions.

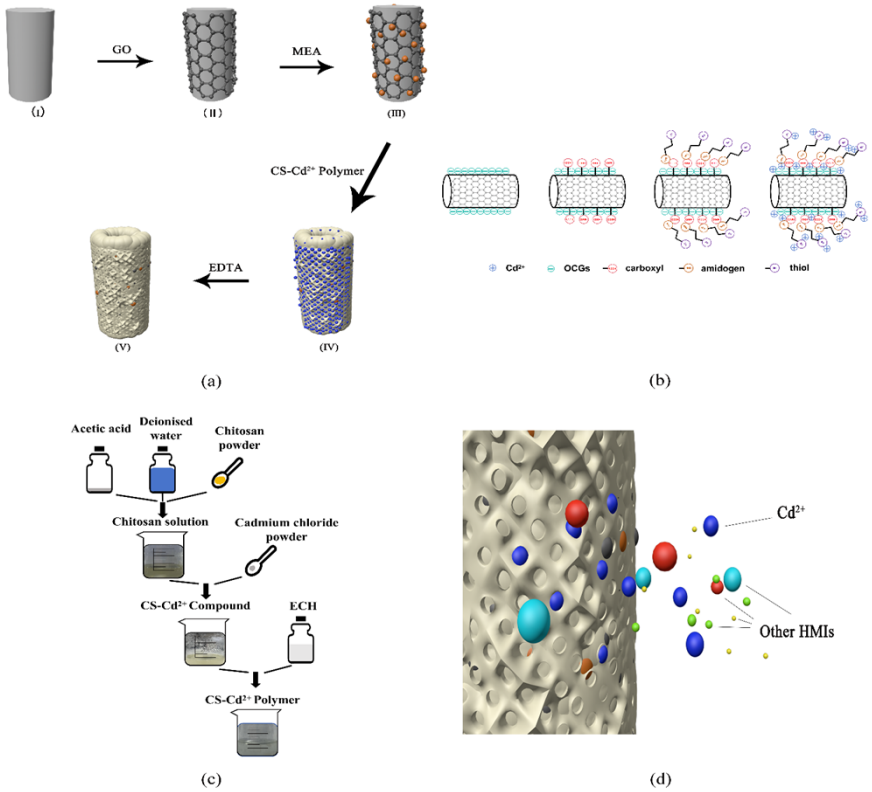

Fig. 5. (a) Sensor functionalization coating process, (b) functionalized schematic of GO-MEA, (c) production process schematic of CS-Cd^{2+}P and (d) ions exchange process between the external solution and functionalized SMNS.

In the second stage, the GO-MEA modified probe was coated with the chitosan-Cd^{2+} polymer (CS-Cd^{2+}P) to accomplish the Cd^{2+}IP. Figure 5(c) illustrates the stages involved in preparing the CS-Cd^{2+}P combination. Initially, a chitosan solution was prepared by blending 2 g of chitosan with 4 ml of acetic acid and 96 ml of DI water and stirring it magnetically overnight for later use. The CS-Cd^{2+} compound was then obtained by adding 0.1 g of cadmium chloride powder

Optics EXPRESS

to the resulting chitosan solution, followed by a magnetic stirring for another four hours. A concentration of 25% ECH was also added to the chitosan-Cd^{2+} solution to synthesize CS-Cd^{2+}P by magnetic stirring, during which the formation was verified as it turned into a bubble-free gel. Finally, the coating process was finalized by dipping the GO-MEA-coated probe into the CS-Cd^{2+}P mixture for 5 mins. This step was continued twice, where the coated fiber dried at 55°C for 2 hours after each cycle. Later, the Cd^{2+} ions were extracted from the polymer layer by cleaning with 0.1 M EDTA, enabling the probe to bind with Cd^{2+} in future sensing. Figure 5(d) illustrates the ions exchange process between the external solution and the GO-MEA and CS-Cd^{2+}IP modified surface of the SMNS interferometer. In contrast, the state of the interference minima at each coating was recorded, as displayed in Fig. 6(a). A variation in both intensity and interference dip was observed after depositing the CS-Cd^{2+}P membrane and extracting the cadmium ions from the coated layer. This effect results from the interaction of the evanescent field of the NCF cladding mode with the coated layers. The coating layer was further authenticated by the scanning electron micrograph (SEM) images in Fig. 6(b). Three identical probes were produced utilizing the coating procedures outlined above, along with the optimal lengths of the MMF and NCF to confirm their reproducibility.

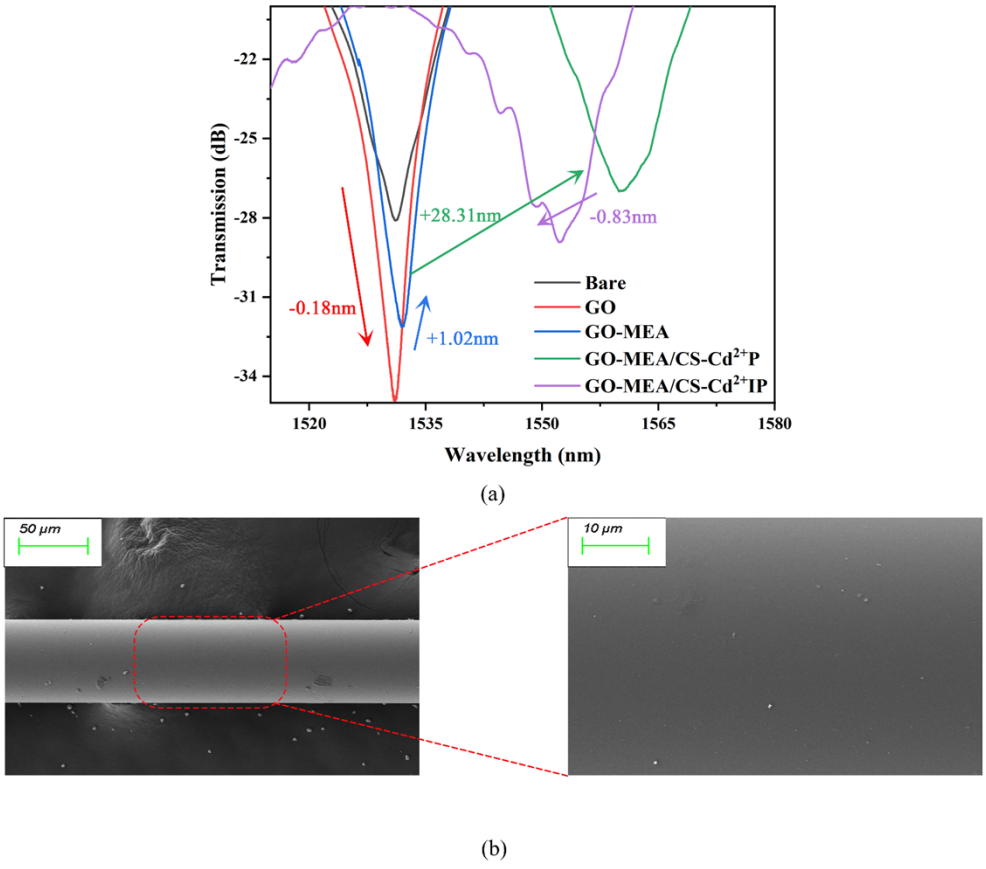

Fig. 6. (a) The recorded interference spectra after each coating step while the sensor was kept in the air and (b) SEM images of GO-MEA/CS-Cd^{2+} IP coated NCF.

Optics EXPRESS

4. Results and discussion

In this section, the sensitivity of the modified SMNS sensor towards Cd^{2+} was analyzed by submerging the fabricated probe into numerous Cd^{2+} aqueous solutions ranging from 0 ppb to 10 ppb. Figure 7(a) displays the response of the fabricated SMNS structure, which was recorded by using the aforesaid experimental setup. It can be noticed that the minima of interference shifted towards the shorter wavelength. This blue movement in wavelength resulted from the formation of bonds between the Cd ions and the GO-MEA coated layer in the presence of carboxylic groups, amino groups and thiol groups in GO-MEA. In addition, each GO-MEA and CS-Cd^{2+}IP coated probe was dipped into various cadmium concentrations by following the above process three times to calculate the average sensitivity. As can be seen from Fig. 7(b), the average sensitivity of three probes was found to be -0.1066 nm/ppb (probe 1), -0.1211 nm/ppb (probe 2) and -0.1063 nm/ppb (probe 3). Besides, probe 2 was chosen for further analysis because of its high sensitivity. The limit of detection (LOD) and limit of quantification (LOQ) of probe 2 was also determined as 0.2824 ppb and 0.9320 ppb based on the equation in [33,34], where σ ($\sigma = 0.0114$) and S denote the standard deviation and the sensitivity of the selected probe.

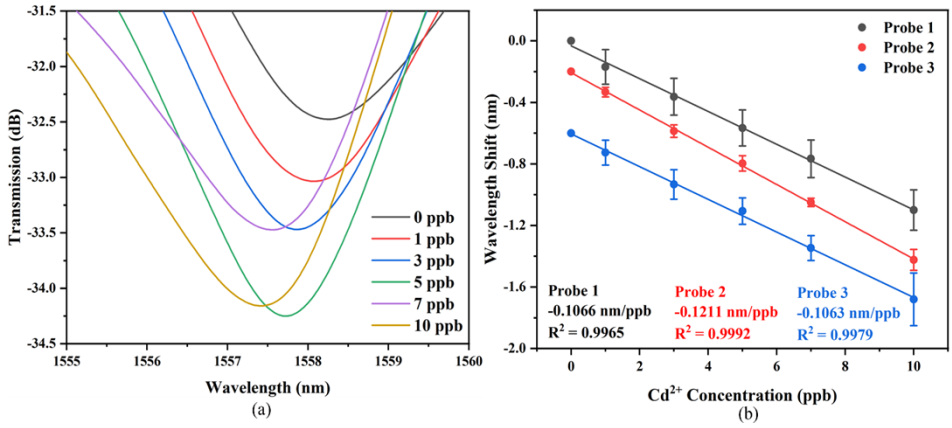

Fig. 7. (a) Shifting in the interference minima (probe 2) measured with different Cd^{2+} concentrations ranging from 0 ppb to 10 ppb and (b) average sensitivity of three modified probes.

The reaction time of the modified sensor corresponding to different cadmium concentrations was examined. The average response time was found to be 90 s while the sensor dipped in 3 ppb, 5 ppb and 10 ppb solutions of Cd^{2+} (illustrated in Fig. 8(a)). Furthermore, in order to validate the condition of the MIT method, the coated SMNS interferometer was then dipped into the EDTA. Upon immersion into the EDTA solution, the spectrum indicated a red shift due to the separation of attached Cd ions from the GO-MEA coated layer, as shown in Fig. 8(b). On the contrary, the binding of cadmium ions with the GO-MEA layer while the coated interferometer was submerged in various Cd^{2+} concentrations led to a blue shift in the interference minima. The interference pattern returned to its initial position after each cycle, thus demonstrating the possibility for reusability (see Fig. 8(b)).

The specificity of the GO-MEA coated SMNS structure has been investigated further by evaluating other heavy metal ion solutions. Following this approach, heavy metal elements such as zinc (Zn^{2+}), copper (Cu^{2+}), mercury (Hg^{2+}) and chromium (Cr^{3+}) with concentrations ranging from 0 ppb to 10 ppb were individually tested to assess the sensor selectivity. It can be noticed from Fig. 9(a) that the proposed sensor is about nine times more sensitive towards cadmium analytes due to the coupling of the target ion and coated membrane. Minimal

Optics EXPRESS

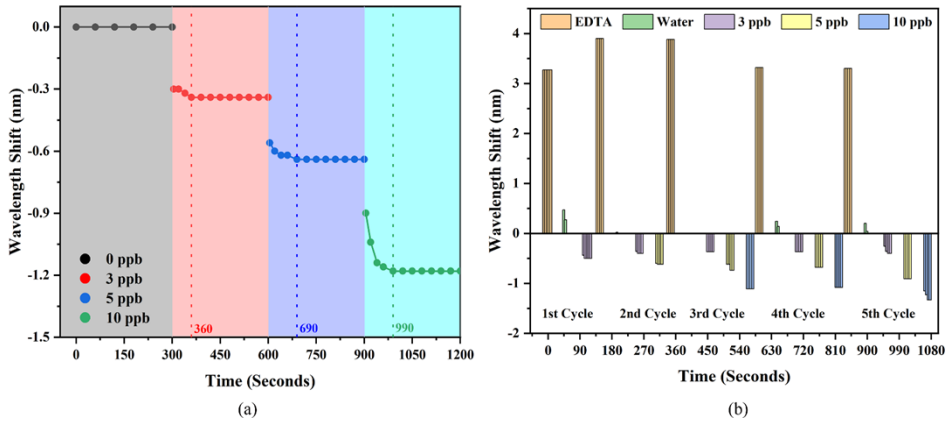

Fig. 8. (a) Response time and (b) reusability of the proposed sensor from 0 ppb to 10 ppb of Cd^{2+} solutions.

wavelength displacement was also spotted when non-template ions were attached to CS via chelation. Subsequently, the response of the fabricated sensor in pH solutions ranging from 5 to 9 was analyzed to enhance the sensor accuracy. Figure 9(b) shows that the interference minima exhibited minor shifts with pH values in the acidic range, where alkaline environments induced significant crosstalk.

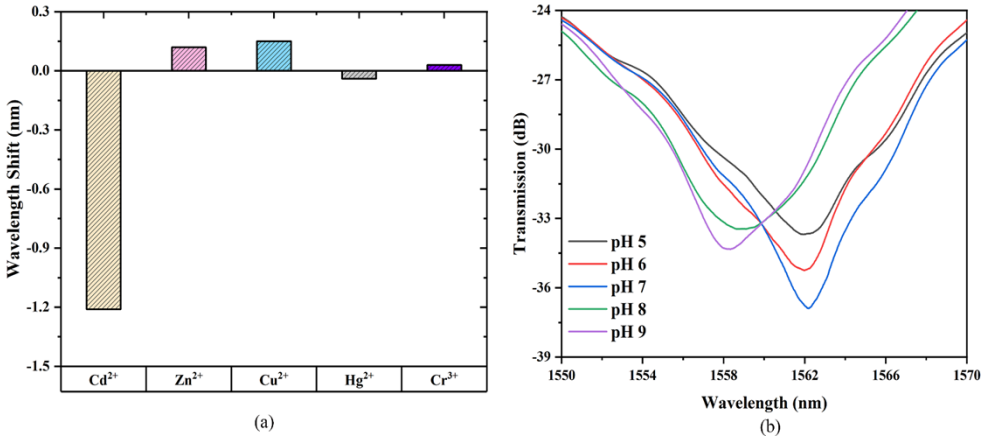

Fig. 9. (a) Selectivity of the proposed Cd^{2+} sensor demonstrated by submerging into various HMI solutions with concentrations from 0 ppb to 10 ppb. (b) Interference movement of the coated sensor was evaluated in pH solutions between 5 to 9.

Following that, the temperature sensitivity of the sensor was measured as it is essential to monitor the sensor response concerning the change in external temperature. An FBG-inscribed SMF was also placed inline with the interferometer to mitigate temperature crosstalk. The temperature sensitivity was evaluated by placing the coated SMNS structure and the FBG in a DI water-contained glass petri dish on a heated plate, with the temperature varied from 25 °C to 50 °C in 5 °C increments. The proposed sensor exhibited a blue shift with increasing temperature, whereas the FBG displayed a red shift, as illustrated in Fig. 10(a) and Fig. 10(b). The responses of both interference spectra and the FBG dip towards temperature change were found to be -0.1818nm/°C and 0.0102 nm/°C, respectively. Combining the SMNS spectra with the change in

Optics EXPRESS

cadmium ions solutions and the temperature sensitivity, the cross-temperature sensitivity was determined to be 1.5012 ppb/°C. Besides, Table 1 summarizes the performance of the proposed sensor alongside existing fiber-optic interferometric sensors for cadmium sensing applications.

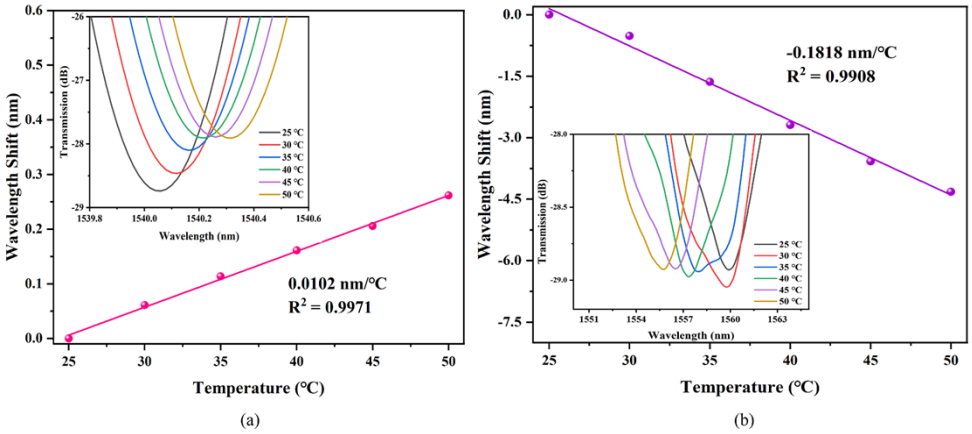

Fig. 10. (a) Transmission spectra shift of the FBG and (b) temperature sensitivity of the coated SMNS interferometer corresponding to ambient temperatures between 25°C and 50°C.

Table 1. Performance of various fiber optic interferometer based sensors for Cd^{2+} detection

Structure	Coated material	Concentration range	Linear sensitivity	LOD	Selectivity	Ref.
U-bent Probe	Gold nanoparticles/ bacteria	0–2 ppb	0.06 a.u./ppb	0.5 ppb	Yes	[35]
Fused-cone SMF	ATU and BIS	0–1350 ppb	4.56×10^{-4} nm/ppb	44.96 ppb	No	[20]
SMF-NCF-PCF-NCF-SMF	SnO_2-MoS_2	0–1.12×10^4 ppb	2.69×10^{-4} nm/ppb	-	Yes	[36]
Three core fiber	PVA/TEOS/ APTES	0–44.96 ppb	0.06 nm/ppb	1.6 ppb	Yes	[21]
SMNS	**GO-MEA/ CS-Cd^{2+} IP**	**0–10 ppb**	**-0.1211 nm/ppb**	**0.2824 ppb**	**Yes**	**this study**

5. Conclusion

A GO-MEA/CS-Cd^{2+}IP functionalized SMNS fiber optic interferometer has been developed for the highly selective detection of Cd^{2+}. The proposed interferometer is constructed by following a sandwich structure, where a 25 mm length of MMF and 25 mm length of NCF have been spliced in between two SMFs. The detection capability of the optimized probes has been examined by varying the refractive indices of the surrounding medium. Besides, the probes have been coated with GO-MEA and CS-Cd^{2+} IP sensing layers using a thermal coating method to increase their specificity towards cadmium ions. By utilizing similar geometrical parameters and coating processes, three probes have been assembled. Among them, the highest sensitivity was found to be -0.1211 nm/ppb within the 0 ppb to 10 ppb cadmium measurement range. The limits of detection and quantification were also recorded as 0.2824 ppb and 0.9320 ppb, respectively, in the same detection area. The sensing reaction time is recorded as 90 s before being stable in

Optics EXPRESS

the concentrations. Furthermore, the sensor has displayed minimal response to other HMIs, showcasing its selective sensing capability for Cd^{2+}. The coated probe has also been found to be pH-insensitive in weakly acidic environments. Additionally, the minima in the spectra have been analyzed to determine the temperature response for both the interferometer-based fiber sensor and the FBG. The thermal sensitivities for the SMNS interferometer and FBG have been measured as -0.1818nm/°C and 0.0102 nm/°C, respectively. Therefore, this sensor offers a simple solution for detecting Cd^{2+} in water-based media and introduces an innovative approach for heavy metal ion sensing applications. Further, the promising results and robustness of the sensor make it suitable for expansion and field applications.

Funding. University Grants Committee (General Research Fund 15209321).

Disclosures. The authors declare no conflicts of interest.

Data availability. No data were generated or analyzed in the presented research.

References

1. A. K. Shakya and S. Singh, "State of the art in fiber optics sensors for heavy metals detection," Opt. Laser Technol. **153**, 108246 (2022).
2. R. Fu, X. Chen, X. Yan, *et al.*, "Optical fiber sensors for heavy metal ion sensing," J. Mater. Sci. Technol. **189**, 110–131 (2024).
3. C. -G. Elinder, L. Friberg, T. Kjellström, *et al.*, " *Biological monitoring of metals*," (World Health Organization, 1994).
4. A. H. Uddin, R. S. Khalid, M. Alaama, *et al.*, "Comparative study of three digestion methods for elemental analysis in traditional medicine products using atomic absorption spectrometry," J. Anal. Sci. Technol. **7**(1), 6–7 (2016).
5. F. B. Alkas, J. A. Shaban, A. A. Sukuroglu, *et al.*, "Monitoring and assessment of heavy metal/metalloid concentration by inductively coupled plasma mass spectroscopy (icp-ms) method in gonyeli lake, cyprus," Environ. Monit. Assess. **189**(10), 516 (2017).
6. G. D. O'Neil, M. E. Newton, and J. V. Macpherson, "Direct identification and analysis of heavy metals in solution (hg, cu, pb, zn, ni) by use of in situ electrochemical x-ray fluorescence," Anal. Chem. **87**(9), 4933–4940 (2015).
7. Q. Ding, C. Li, H. Wang, *et al.*, "Electrochemical detection of heavy metal ions in water," Chem. Commun. **57**(59), 7215–7231 (2021).
8. Y. Shen, X. Gao, H.-J. Lu, *et al.*, "Electrochemiluminescence-based innovative sensors for monitoring the residual levels of heavy metal ions in environment-related matrices," Coordin. Chem. Rev. **476**, 214927 (2023).
9. B. Bansod, T. Kumar, R. Thakur, *et al.*, "A review on various electrochemical techniques for heavy metal ions detection with different sensing platforms," Biosens. Bioelectron. **94**, 443–455 (2017).
10. Y.-n. Zhang, Y. Sun, L. Cai, *et al.*, "Optical fiber sensors for measurement of heavy metal ion concentration: A review," Measurement **158**, 107742 (2020).
11. A. Al Noman, J. N. Dash, X. Cheng, *et al.*, "Pcf based modal interferometer for lead ion detection," Opt. Express **30**(4), 4895–4904 (2022).
12. M.-F. Liu, J.-W. Wang, and S.-J. Hwang, "In-fiber mach-zehnder interferometer based on hollow optic fiber for metal ion detection," Opt. Express **30**(15), 26006–26017 (2022).
13. M. Yan, R. Wang, B. Liu, *et al.*, "Layer by layer assembly cs/paa for high sensitivity detection of heavy metal ions using mode interference sensor," Opt. Commun. **545**, 129725 (2023).
14. Y. Wing Fen and W. M. M. Yunus, "Surface plasmon resonance spectroscopy as an alternative for sensing heavy metal ions: A review," Sensor Rev. **33**(4), 305–314 (2013).
15. Z. Yan, Y. Cai, J. Zhang, *et al.*, "Fluorescent sensor arrays for metal ions detection: A review," Measurement **187**, 110355 (2022).
16. L. Guerrini and R. A. Alvarez-Puebla, "Surface-enhanced raman scattering sensing of transition metal ions in waters," ACS Omega **6**(2), 1054–1063 (2021).
17. D. Lyu, Q. Huang, X. Wu, *et al.*, "Optical fiber sensors for water and air quality monitoring: A review," Opt. Eng. **63**(3), 031004 (2024).
18. A. A. Noman, J. N. Dash, X. Cheng, *et al.*, "Mach-zehnder interferometer based fiber-optic nitrate sensor," Opt. Express **30**(21), 38966–38974 (2022).
19. A. Miliou, "In-fiber interferometric-based sensors: Overview and recent advances," Photonics **8**(7), 265 (2021).
20. Z. Pan, J. Feng, X. Hu, *et al.*, "High sensitivity fiber sensor for measurement of cd 2 + concentration in aqueous solution based on reflective mach-zehnder interference with temperature calibration," Opt. Express **27**(22), 32621–32629 (2019).
21. S. Xie, Y. Liu, H. Chen, *et al.*, "Trace cadmium ion detection using optical fiber mach–zehnder interferometer coated with pva/teos/aptes," Z. Naturforsch. A **77**(12), 1217–1222 (2022).
22. H. Li, Q. Tu, Z. Zhang, *et al.*, "An asymmetric stns-mzi structure and its applications in temperature and cd2 + monitoring," Opt. Fiber Technol. **88**, 103987 (2024).

Optics EXPRESS

23. M. Li, C. Feng, M. Li, *et al.*, "Synthesis and characterization of a surface-grafted cd (ii) ion-imprinted polymer for selective separation of cd (ii) ion from aqueous solution," Appl. Surf. Sci. **332**, 463–472 (2015).
24. L. Yu, L. Sun, Q. Zhang, *et al.*, "Nanomaterials-based ion-imprinted electrochemical sensors for heavy metal ions detection: A review," Biosensors **12**(12), 1096 (2022).
25. P. M. S. Tchekwagep, R. D. Crapnell, C. E. Banks, *et al.*, "A critical review on the use of molecular imprinting for trace heavy metal and micropollutant detection," Chemosensors **10**(8), 296 (2022).
26. Y. Bian, Z.-Y. Bian, J.-X. Zhang, *et al.*, "Effect of the oxygen-containing functional group of graphene oxide on the aqueous cadmium ions removal," Appl. Surf. Sci. **329**, 269–275 (2015).
27. N. Tang, C.-G. Niu, X.-T. Li, *et al.*, "Efficient removal of cd2 + and pb2 + from aqueous solution with amino-and thiol-functionalized activated carbon: Isotherm and kinetics modeling," Sci.Total Environ. **635**, 1331–1344 (2018).
28. P. Zaca-Morán, J. Padilla-Martínez, J. Pérez-Corte, *et al.*, "Etched optical fiber for measuring concentration and refractive index of sucrose solutions by evanescent waves," Laser Phys. **28**(11), 116002 (2018).
29. Y. Zhao, J. Zhao, and Q. Zhao, "Review of no-core optical fiber sensor and applications," Sens. Actuators A Phys. **313**, 112160 (2020).
30. S. Xu, S. Liu, J. Guan, *et al.*, "Refractometer based on extinction ratio demodulation using no-core and dispersion-compensating fiber structure," Opt. Commun. **553**, 130067 (2024).
31. Z. Rui, Z. Xiang, F. Zeng, *et al.*, "Liquid level sensor with high sensitivity based on hetero core structure," IEEE Sensors J. **22**(14), 14051–14057 (2022).
32. K. Xiong, Q. Fan, T. Wu, *et al.*, "Enhanced bovine serum albumin absorption on the n-hydroxysuccinimide activated graphene oxide and its corresponding cell affinity," Mat. Sci. Eng. C-mater. **81**, 386–392 (2017).
33. A. A. Noman, J. N. Dash, M. A. A. Maruf, *et al.*, "Label-free DNA detection using etched tilted bragg fiber grating-based biosensor," Sensors **23**(16), 7019 (2023).
34. H. A. Leslie, M. J. Van Velzen, S. H. Brandsma, *et al.*, "Discovery and quantification of plastic particle pollution in human blood," Environ. Int. **163**, 107199 (2022).
35. P. Halkare, N. Punjabi, J. Wangchuk, *et al.*, "Bacteria functionalized gold nanoparticle matrix based fiber-optic sensor for monitoring heavy metal pollution in water," Sens. Actuators B Chem. **281**, 643–651 (2019).
36. H. Chen, X. Yang, and W. Feng, "Cadmium-ion detection: A comparative study for a sno 2, mos 2, sno 2/mos 2, sno 2-mos 2 sensing membrane combination with a fiber-optic mach–zehnder interferometer," Appl. Opt. **60**(4), 799–804 (2021).